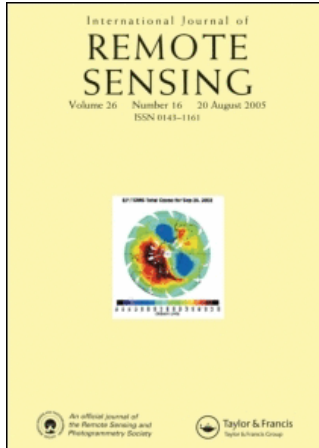


This article was downloaded by:[Universite De Sherbrooke]
On: 28 July 2008
Access Details: [subscription number 793218015]
Publisher: Taylor & Francis
Informa Ltd Registered in England and Wales Registered Number: 1072954
Registered office: Mortimer House, 37-41 Mortimer Street, London W1T 3JH, UK



International Journal of Remote Sensing

Publication details, including instructions for authors and subscription information:
<http://www.informaworld.com/smpp/title-content=t713722504>

Advances in seasonal snow water equivalent (SWE) retrieval using **in situ** passive microwave measurements over first-year sea ice

A. Langlois^a, D. G. Barber^a

^a Centre for Earth Observation Science (CEOS), University of Manitoba, Winnipeg, Manitoba, Canada

Online Publication Date: 01 January 2008

To cite this Article: Langlois, A. and Barber, D. G. (2008) 'Advances in seasonal snow water equivalent (SWE) retrieval using **in situ** passive microwave measurements over first-year sea ice', International Journal of Remote Sensing, 29:16, 4781 — 4802

To link to this article: DOI: 10.1080/01431160801908145
URL: <http://dx.doi.org/10.1080/01431160801908145>

PLEASE SCROLL DOWN FOR ARTICLE

Full terms and conditions of use: <http://www.informaworld.com/terms-and-conditions-of-access.pdf>

This article maybe used for research, teaching and private study purposes. Any substantial or systematic reproduction, re-distribution, re-selling, loan or sub-licensing, systematic supply or distribution in any form to anyone is expressly forbidden.

The publisher does not give any warranty express or implied or make any representation that the contents will be complete or accurate or up to date. The accuracy of any instructions, formulae and drug doses should be independently verified with primary sources. The publisher shall not be liable for any loss, actions, claims, proceedings, demand or costs or damages whatsoever or howsoever caused arising directly or indirectly in connection with or arising out of the use of this material.

Advances in seasonal snow water equivalent (SWE) retrieval using *in situ* passive microwave measurements over first-year sea ice

A. LANGLOIS* and D. G. BARBER

Centre for Earth Observation Science (CEOS), University of Manitoba, 125 Dysart Rd,
Winnipeg, Manitoba, Canada

(Received 19 April 2007; in final form 17 December 2007)

Dramatic changes have occurred in the Arctic over the past three decades in response to an accelerated warming that will have a significant impact on the world's climate. Snow accumulation (measured as snow water equivalent, SWE) over sea ice plays a key role in the changes observed due to its effect on the surface energy balance that dictates the timing of sea-ice freeze-up and decay. Increased awareness of the role of snow in the Arctic system has triggered numerous studies that have attempted to characterize snow accumulation from space since the early 1980s, but none has successfully quantified SWE on a seasonal basis.

This work presents the first seasonally valid SWE algorithm for first-year sea ice based on *in situ* passive microwave radiometry. The *in situ* data were collected as a part of the Canadian Arctic Shelf Exchange Study (CASES) during the overwintering mission of the Canadian Coast Guard Ship (CCGS) Amundsen in 2003–2004. Previous work clearly demonstrated two different patterns of seasonal snow evolution, for which the algorithm presented in this paper accounts for. Our algorithm's results are valid for temperatures between -5 and -30°C and SWE in the range of 0–55 mm. Results show that the behaviour of the snow's thermophysical properties and brightness temperatures (T_b) is quite different in the winter cooling period compared with that in the warming period, where temperature gradient metamorphism begins at a SWE value of 33 mm. The SWE algorithm successfully models this change with a high degree of correlation.

1. Introduction

A dramatic climate response to increasing global temperatures – a reduction in sea-ice volume – has been observed recently in the Arctic (ACIA 2004, IPCC 2001). Sea-ice depletion of approximately 7.8% per decade since the 1970s has decreased the total sea-ice coverage by more than 1.3 million km^2 (Francis *et al.* 2005, Stroeve *et al.* 2005). Of particular concern is the decrease in thickness measured in both first-year and multi-year ice. The 32% decrease in thick ice volume measured between 1958 and 1997 (Yu *et al.* 2004) can have a significant impact on global-scale climate variability due to its effect on atmospheric circulation patterns (Gerdes 2006) such as the North Atlantic Oscillation (Polyakov *et al.* 2003). Current sea-ice thickness models (Martin *et al.* 2005) have lingering uncertainties due to strong assumptions with regards to snow cover. Changes in sea-ice/snow thickness and spatial extent affect a variety of strong

*Corresponding author. Email: A.Langlois2@USherbrooke.ca

feedback mechanisms such as the ice-albedo feedback (Curry *et al.* 1996, Holland and Bitz 2003), which controls the timing of sea-ice freeze-up and decay (e.g. Eicken 2003).

Snow cover plays an important role in the global Arctic energy budget due to its effect on radiative, gas and mass transfers between the ocean and the atmosphere (e.g. Grenfell and Maykut 1977, Ledley 1991, Serreze *et al.* 2003). The low thermal conductivity and diffusivity of snow limit the release of latent heat from the underlying growing sea ice, thus controlling seasonal ice thickness (Warren *et al.* 1999, Sturm *et al.* 2002, Eicken 2003). With the recent ice depletion recorded over the past three decades, it becomes even more essential to adequately quantify the impact of snow over sea ice in order to more accurately forecast the future state of the cryosphere. Satellite remote sensing provides the most promising tool to assess global snow cover extent and thickness needed in climate models (Stroeve *et al.* 2005, Barber and Hanesiak 2004, Francis *et al.* 2005, Rothrock and Zhang 2005), but accurate methods of interpreting the satellite signal have yet to be developed (Kelly *et al.* 2003, Langlois *et al.* 2007b).

The most common approach in estimating snow thickness over Arctic sea ice is to calculate snow water equivalent (SWE). In past experiments, only limited work was conducted over first-year sea ice (Drobot and Barber 1998, Cavalieri and Comiso 2000, Barber *et al.* 2003, Markus *et al.* 2006, Langlois *et al.* 2007b) due to logistical constraints, which limited most of the work to the spring season. Snow properties over sea ice behave quite differently than over land, but their impact on climate is also significant (Powell *et al.* 2006). Passive microwave remote sensing represents a powerful tool in SWE studies due to the importance of snow scattering effects at high frequencies with respect to dielectric properties (Tsang and Kong 1992, Singh and Gan 2000). The majority of land algorithms are based on the brightness temperature difference between 19 and 37 GHz ($\Delta T_{bP19-37}$) where the snow cover extent and depth can be extracted based on multi-regression analysis (e.g. Chang *et al.* 1982, Singh and Gan 2000). Recent results showed that this concept ($\Delta T_{bP19-37}$) might not be optimal over sea ice due to the relatively thinner snowpack, resulting in high uncertainties in derived SWE. Improved results were observed using a single-frequency algorithm (Barber *et al.* 2003, Langlois *et al.* 2007b) in agreement with work by Armstrong and Brodzik (2001) and Foster *et al.* (2005), who originally suggested using single-frequency/polarization algorithms.

The development of SWE retrieval algorithms over sea ice is still in its infancy. To constrain our analysis, we focus on three primary objectives. We want to (a) evaluate the impact of seasonally evolving snow cover on *in situ* passive microwave signatures, (b) develop a seasonal SWE algorithm valid over the typical range of seasonal snow thickness and temperatures, and (c) compare this algorithm with recent *in situ* and satellite products.

2. Methods

The data provided in this study were collected during the Canadian Arctic Shelf Exchange Study (CASES) overwintering mission. The Canadian Coast Guard Ship (CCGS) Amundsen was purposely frozen into a pan of smooth first-year sea ice in proximity to the various sampling sites (coordinates: 126.30°W, 70.03°N on figure 1). The pan was located approximately 20 km offshore of Franklin Bay, Northwest Territories. Further details on the study location can be found in Langlois *et al.* (2007a,b). The study period started on 10 December 2003 (day 344) and ended on 7 May 2004 (day 127).

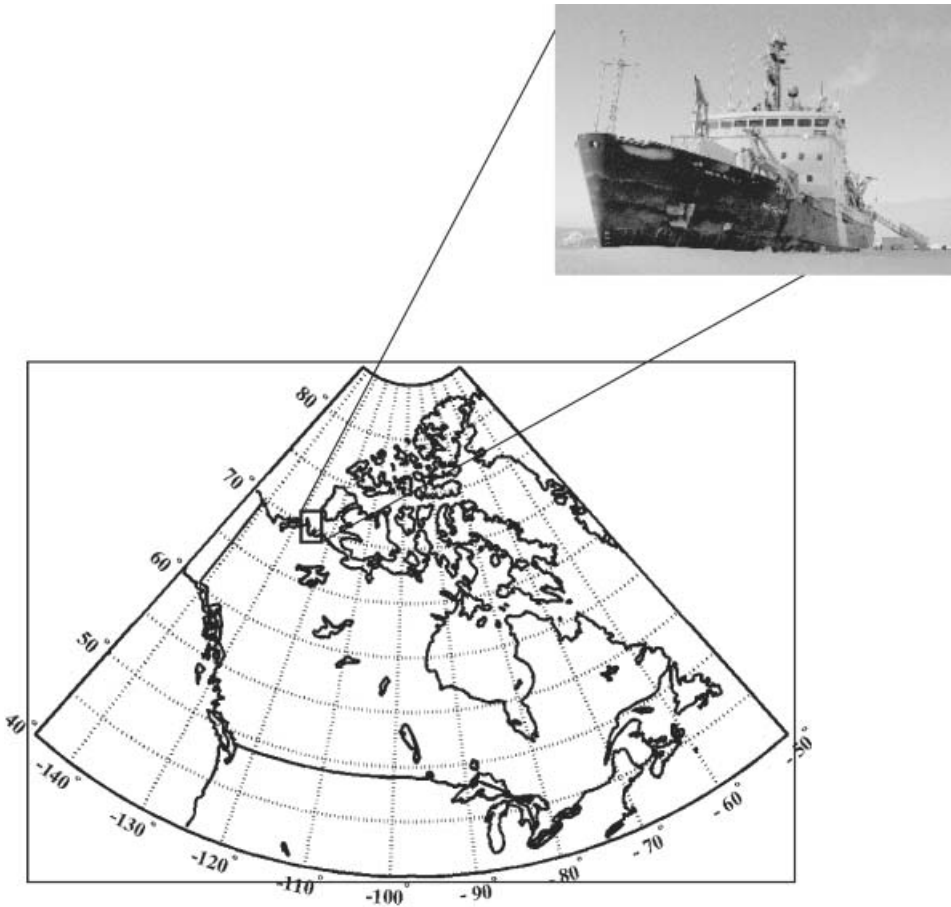


Figure 1. Study site location.

2.1 Snow physical and electrical data

Basic meteorological data (air temperature, wind speed, and direction) were measured on a daily basis using the AXYS Automated Voluntary Observation Ship (AVOS) system mounted on the roof of the Amundsen. Snow physical data were collected over a dedicated snow sampling area, which was undisturbed for the duration of the study. Snow pits were excavated to measure thickness, SWE, density, temperature, salinity, wetness and grain size. Samples were taken at a 2-cm vertical resolution, three times a day every second day between 10 December 2003 and 7 May 2004. The snow covers were separated in different layers (L) based on visual interpretation. At the beginning of the sampling period, snow was characterized by four distinct layers (L1 to L4), and evolved in thickness up to eight layers (L1 to L8). We conducted a Tukey *post hoc* ANOVA statistical test to determine if these layers were statistically different from one another throughout the sampling period. Results showed that all layers were statistically different for at least two snow physical properties with 95% confidence intervals. Complete details on the snow sampling can be found in Langlois *et al.* (2007a).

Permittivity (ϵ') and dielectric loss (ϵ'') of snow over first-year sea ice can be calculated from a dielectric mixture model (Barber and Thomas 1998, Barber *et al.*

2003) of the form proposed by Polder-Van Santen and later modified by de Loor (Ulaby *et al.* 1986) using snow wetness, density, temperatures, and salinity measurements. Wetness below 1% is considered 'dry' and brine is treated as an 'inclusion dielectric' within a dry snow 'host dielectric' (after Mätzler 1987 and Drinkwater and Crocker 1988). Wetness above 1% is considered 'wet' and water is treated as an 'inclusion dielectric' within a dry snow 'host dielectric'. See Barber *et al.* (1995) for further details on snow electrical calculations.

2.2 Brightness temperatures

The surface-based radiometer (SBR) was mounted on the port side of the Amundsen, approximately 13 m above the snow surface. At an incidence angle of 53° (Brewster angle), the field of view was approximately $12\text{ m} \times 12\text{ m}$. The radiometer used in this study includes 19 and 37 GHz antennas (Asmus and Grant 1999) in both horizontal (h-pol) and vertical (v-pol) polarizations. Each SBR measurement consisted of 5 min exposure of the antennas. Calibrations were conducted on a weather-dependent basis using a foam-type blackbody as the hot source and the sky as the cold source. Further information on the calibration and precision of the radiometers is available elsewhere (Asmus and Grant 1999).

3. Results

3.1 Micrometeorological data

The seasonal evolution of air temperatures followed a typical winter pattern (figure 2(a)) distinguished by a cooling and a warming period. The minimum temperature (-37.9°C) was measured on day 58. Throughout the season, values oscillated between -15 and -34°C with larger variations measured during the cooling period. Daily averaged wind speed remained under 20 m s^{-1} until day 94 when a series of strong wind events began and lasted until the end of the sampling period (figure 2(b)). Winds over 12 m s^{-1} were measured on days 5 (12.4 m s^{-1}), 19 (15.49 m s^{-1}), 42 (12.19 m s^{-1}), 62 (13.27 m s^{-1}) and 83 (12.55 m s^{-1}). These winds were accompanied by snowfalls that increased snow thickness (figure 3). Total cloud amount was variable throughout the studied period with average coverage values of 3.28 and 2.72 octas for the cooling and warming periods, respectively (Fisico 2005). Generally, the cloud cover and opacity were higher in the autumn prior to day 345 and spring after day 115 (figure 2(c)).

The net radiation budget (Q^*) remained negative until day 91 when the first positive values were measured (figure 2(d)). Q^* varied between 0 and -45 W m^{-2} , with an average of -27 W m^{-2} . The average increased to -9 W m^{-2} between day 91 and 127, coincident with a significant increase in both downwelling shortwave and longwave radiation budgets.

3.2 Snow evolution and brightness temperatures

In the radiometer's field of view at an incidence angle of 53° , the snow thickness (figure 3) evolved from 6 to 8 cm between days 344 and 5 (Cluster 1), 16–17 cm between days 6 and 42 (Cluster 2), 26–42 cm between days 43 and 91 (Cluster 3), and 64–77 cm between days 92 and 127 (Cluster 4). When plotted against brightness temperatures, we note that the brightness temperatures at 19 and 37 GHz are quite sensitive to changes in snow thickness (figure 4). The cluster analysis gave four

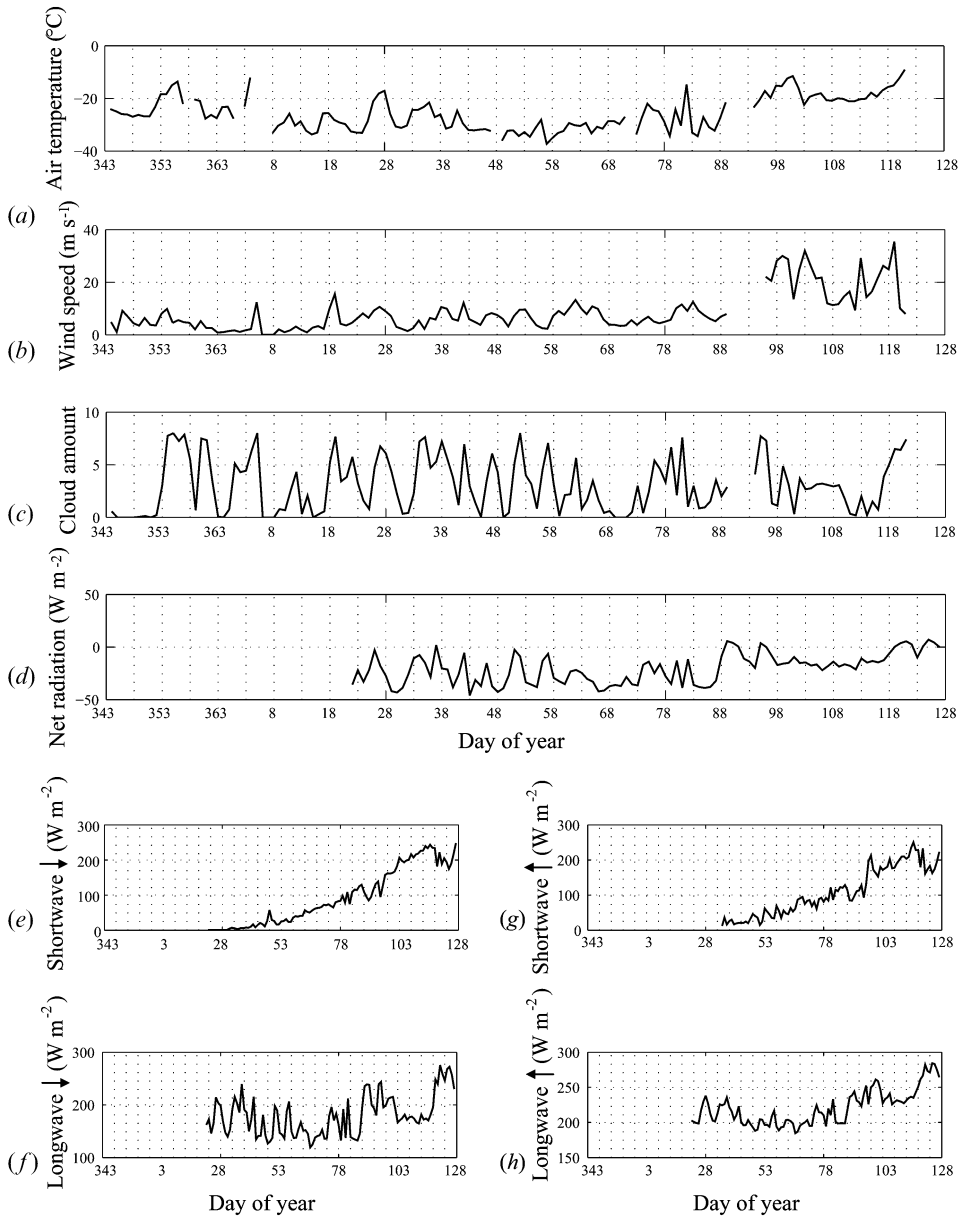


Figure 2. Temporal evolution of (a) air temperatures ($^{\circ}\text{C}$), (b) wind speed (m s^{-1}), (c) cloud amount (octas), (d) net radiation (W m^{-2}), (e) incoming shortwave radiation (W m^{-2}), (f) incoming longwave radiation (W m^{-2}), (g) reflected shortwave radiation (W m^{-2}) and (h) upwelling longwave radiation (W m^{-2}). All x-axes represent day of year.

significantly different groups corresponding to measured variations in SWE. The first increase measured on day 5 caused T_b to increase at both frequencies. The second and third snowfalls on days 42 and 91 caused the brightness temperatures to decrease until the end of the sampling period (figure 4). A k -means cluster analysis showed that these groups are significantly distinct at both 19 and 37 GHz with a mean distance value of 0.9, with the exception of three data points in Cluster 3.

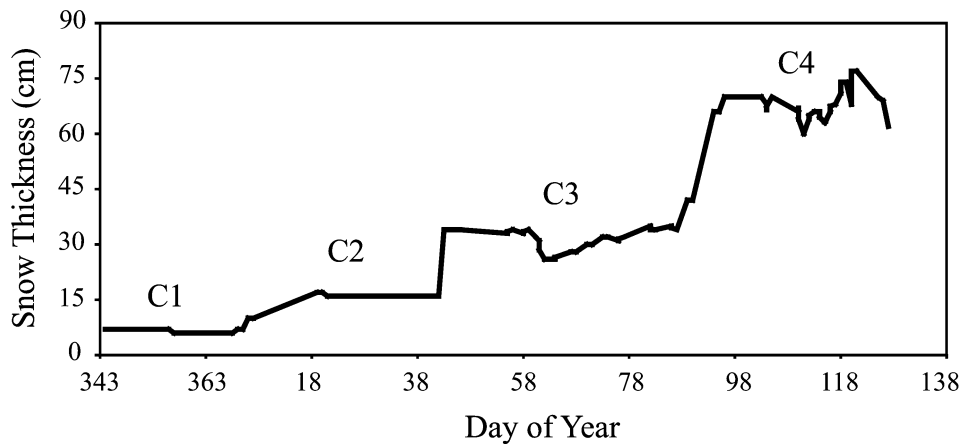


Figure 3. Temporal evolution of snow thickness (cm).

Thermophysical, electrical and brightness temperatures are shown in figures 5–9 and a detailed description of their temporal evolution follows in §3.2.1–3.2.4.

3.2.1 Cluster 1 (C1). During this period, snow grain size was on average 3, 2.6 and 2.4 mm² for L1, L2 and L3, respectively (figure 5(a)), whereas snow density at L2 increased slightly, from 250 to 275 kg m⁻³ to over 300 kg m⁻³ (figure 5(b)). Volume temperatures decreased overall with the exception of a peak measured at all three layers between days 353 and 357 (increase from an average of -18.4 to -9.8°C in figure 6(a)) in response to a passing weather system. Minimum values were recorded on day 2 at -18.7, -21.6 and -22.3°C for L1, L2 and L3, respectively. Furthermore, maximum salinity values were recorded at the beginning of this period for all layers (figure 7(a)). A desalination rate of approximately 0.74 ppt day⁻¹ (where ‘ppt’ denotes parts per thousand) was then measured at L1 and L2 until day 5. Brine volume behaved accordingly with a significant decrease in L1 from 8% to 2% (figure 7(b)). Due to a lack of input data for the dielectric model, no permittivity or dielectric loss values are available during this period.

Brightness temperatures (T_b) for both 19 and 37 GHz increased between days 348 and 357 where T_b reached 259, 260 and 266 K, respectively, in the vertical polarization (figure 8); values of 247, 252 and 263 K were measured in the horizontal polarization. The depolarization ($T_{bV} - T_{bH}$) decreased between day 355 and 361 for both 19 and 37 GHz (17–3 K at 19 GHz).

3.2.2 Cluster 2 (C2). At the beginning of this period, snow thickness increased from an average of 7 cm to 16 cm. Minimum grain size was measured at 1.4 mm² and 1.2 mm² for L2 and L3 (figure 5(a)) while averaged snow density increased for both L2 (+66 kg m⁻³) and L3 (+60 kg m⁻³) (figure 5(b)). Minimum temperatures were reached on days 31 and 41 (< -20°C at all layers in figure 6(a)). Low salinity values were measured throughout the period (figure 7(a)) and the lowest brine volume values were measured during C2 for L2 and L3 with a minimum below 0.5% (figure 7(b)). As with C1, very few permittivity or dielectric loss values are available during this period due to a lack of input data for the dielectric model.

Brightness temperatures did increase between day 6 and 19 to 276 K for both 19 and 37 GHz in the v-pol (figure 8). The increase, to values of 259 and 262 K,

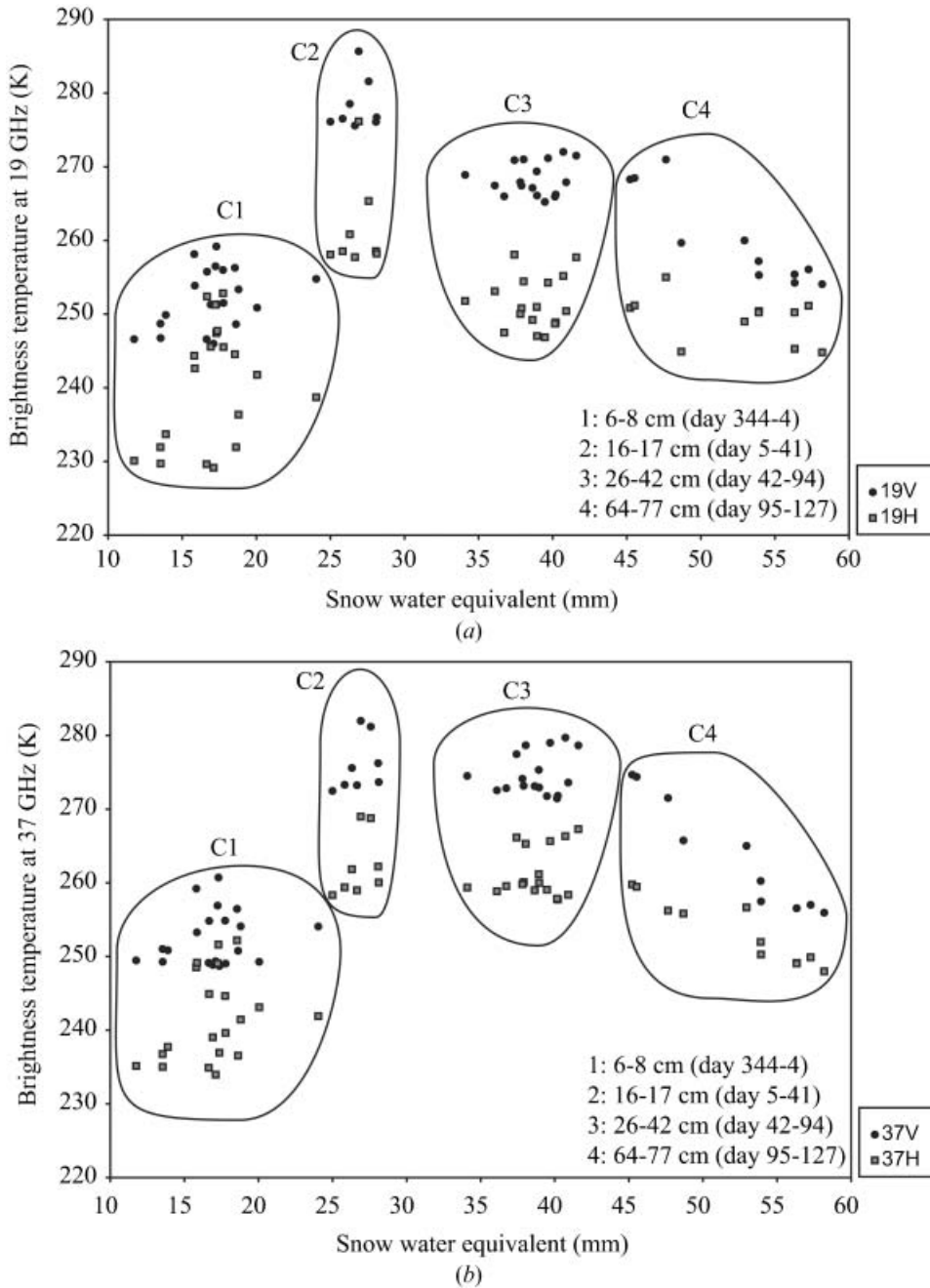


Figure 4. Relationship between brightness temperatures and evolving snow water equivalent (SWE) for (a) 19 GHz and (b) 37 GHz.

respectively, was slightly smaller in h-pol. Values remained high until day 37 when the maximum seasonal values were reached at all frequencies and polarizations (286 and 282 K in the v-pol and 276 and 269 in the h-pol). The overall increase during C2 corresponds to 0.32 and 0.27 K day^{-1} for 19 GHz and 0.56 and 0.49 K day^{-1} for

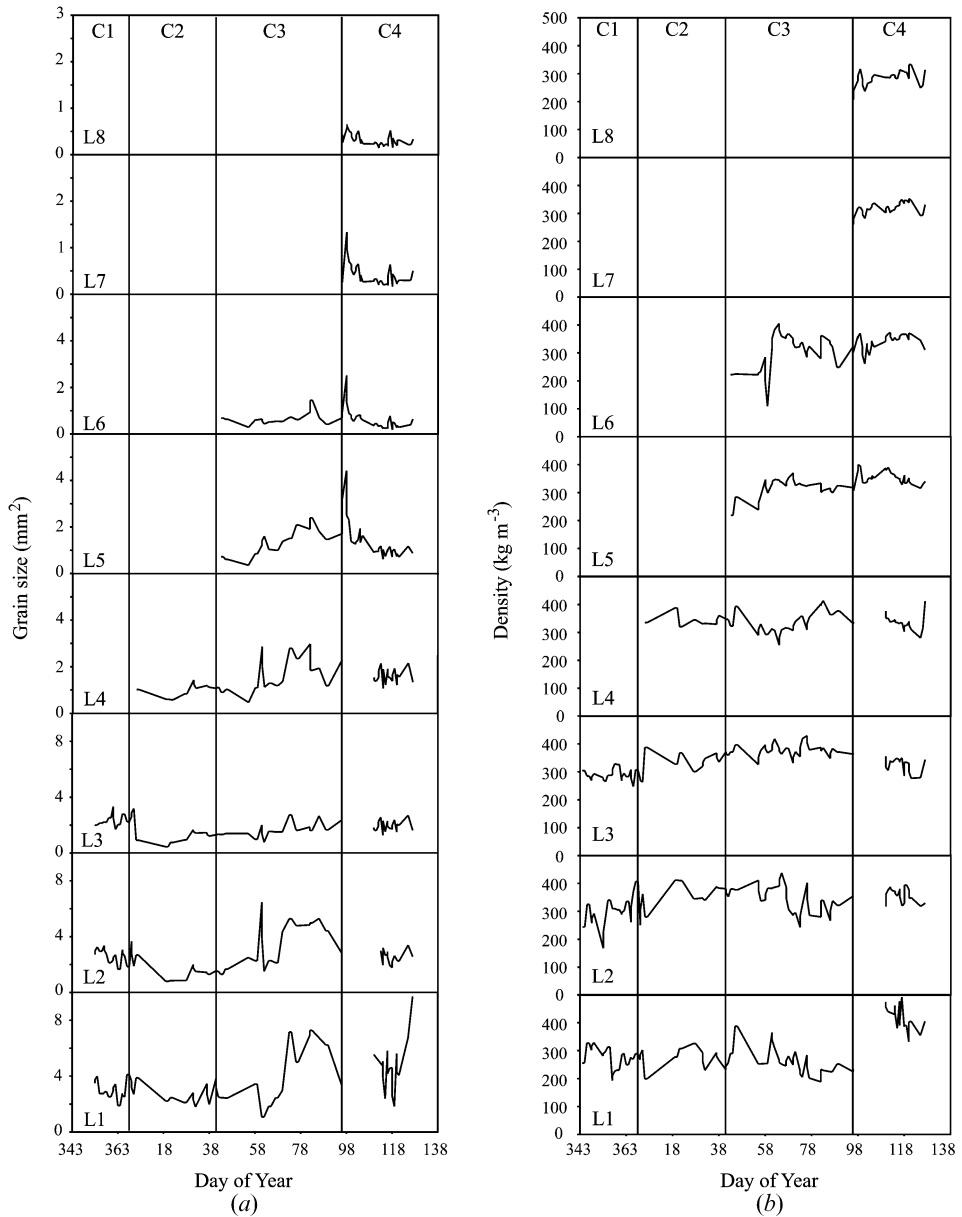


Figure 5. Temporal evolution of (a) snow grain size (mm^2) and (b) density (kg m^{-3}).

37 GHz in the v-pol and h-pol, respectively. The depolarization values remained very stable for 19 and 37 GHz where the average values were 16.7 and 13.6 for 19 and 37 GHz, respectively.

3.2.3 Cluster 3 (C3). Snow grain size increased significantly at all layers during this period (figure 5(a)), reaching their maximum values for the winter season. Grain size varied between 5 and 7 mm^2 for L1 and L2 and just below 3 mm^2 for L3 and L4. Snow density decreased slightly at L1 and L2 while increasing for L5 and L6 (figure 5(b)). The volume temperatures increased in all layers at the start of C3 (figure 6(a)) and the

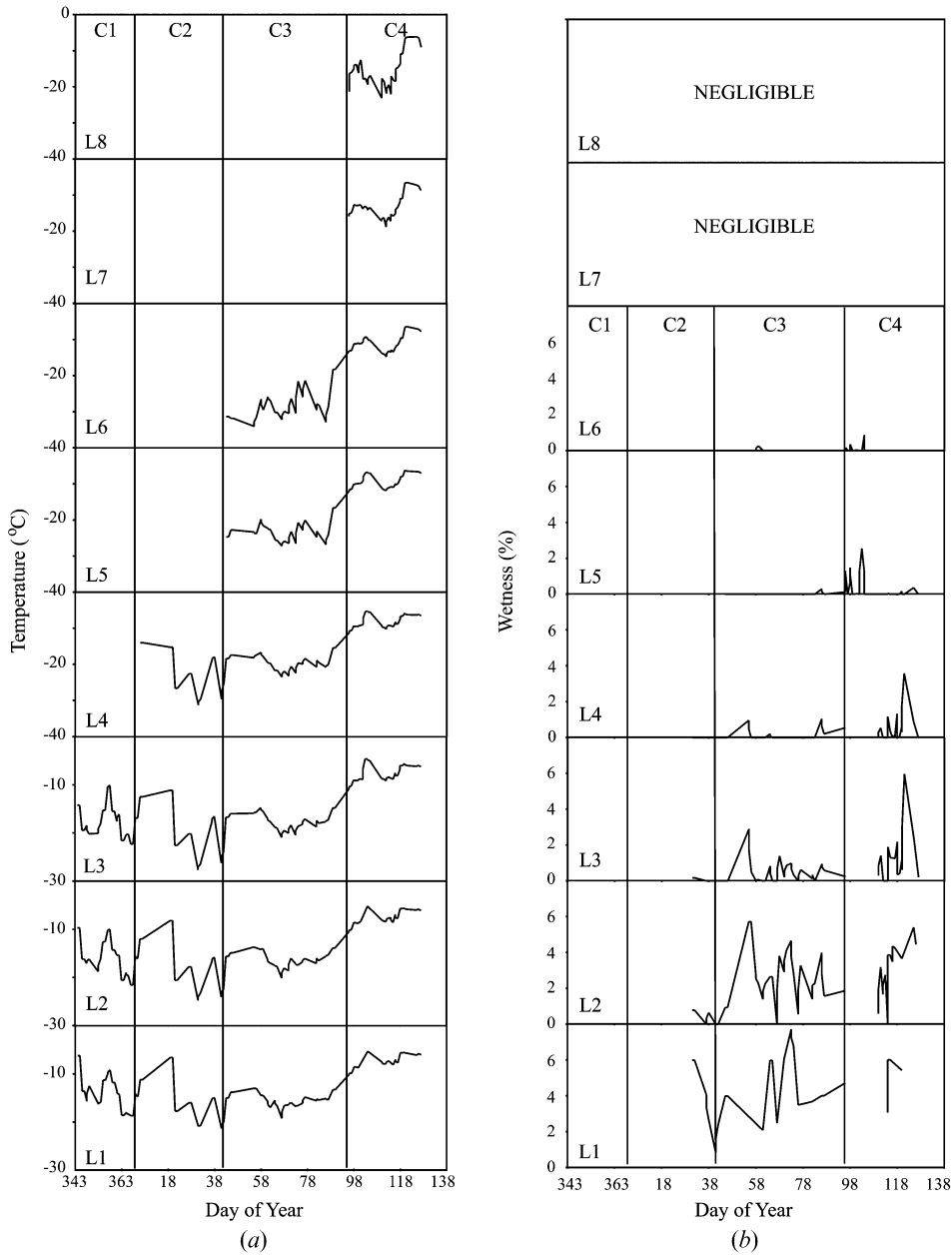


Figure 6. Temporal evolution of (a) temperatures ($^{\circ}\text{C}$) and (b) wetness (%).

first measurements of wetness also occurred during this period (figure 6(b)) with values scattered between 0 and 6% for L1 and L2, and from 0 to 2% for L3. No significant trend was measured in salinity and brine volume (figure 7(a) and (b)).

Snow permittivity (ϵ') oscillated between 1.5 and 2 between days 42 and 91 in all layers (figure 9(a)). The lowest values were modelled between days 42 and 60 in L5 and L6 ($\epsilon' < 1.5$). The most important variations were measured at L1 and L2 when a noticeable decrease between days 60 and 70 reduced the average permittivity from

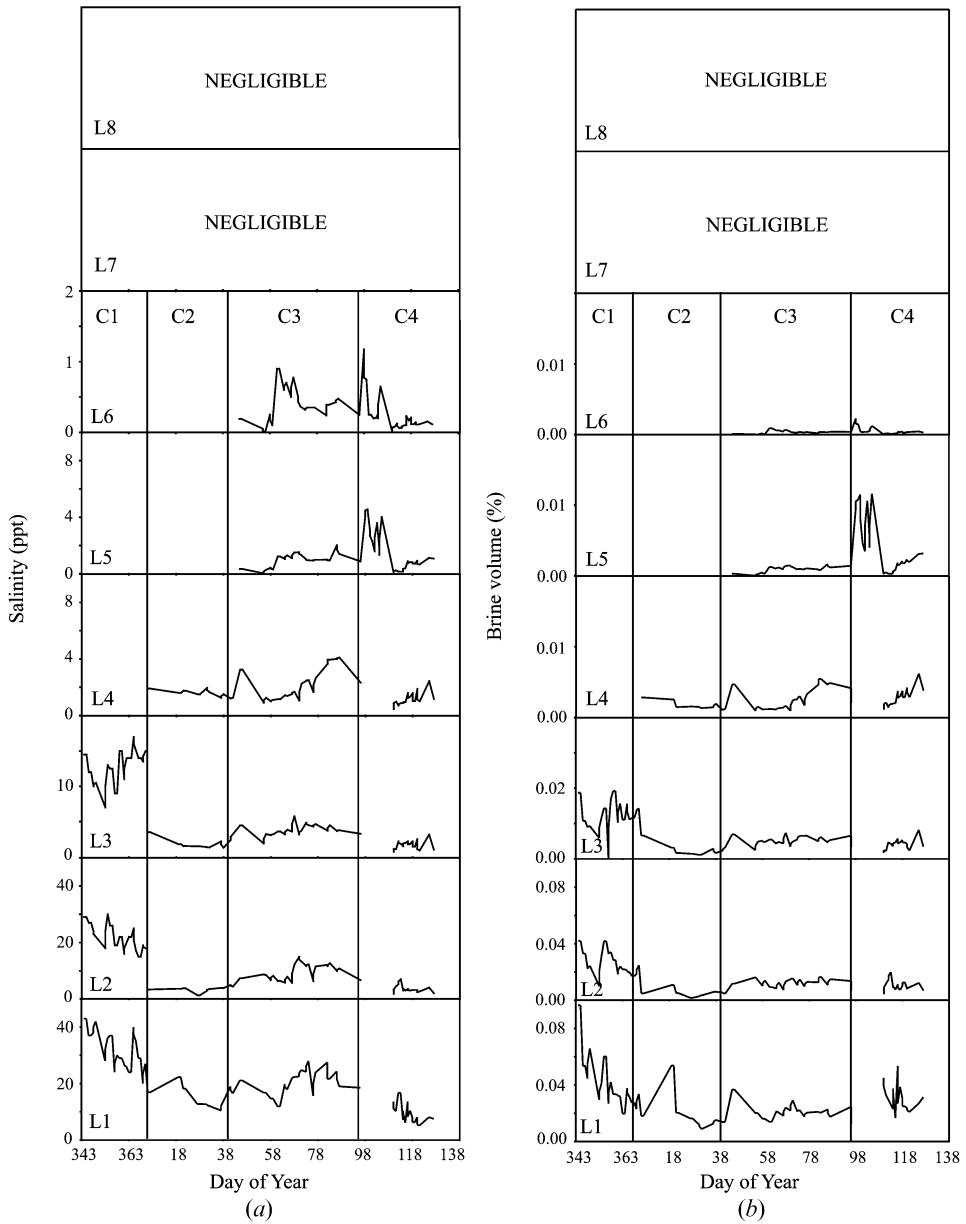


Figure 7. Temporal evolution of (a) salinity (ppt) and (b) brine volume (%).

1.8 to 1.5. The dielectric loss (ϵ'') values were negligible from L3 through L8 (figure 9(b)). Higher values of dielectric loss were measured at L1 and L2, reaching 0.47 and 0.26, respectively.

The brightness temperature, T_b , did not vary greatly at 19 and 37 GHz (figure 8), though a sharp increase then decrease was observed between days 76 and 82 at all frequencies and polarizations. This increase amounted to 6–11 K at both 19 and 37 GHz. Interestingly, the depolarization remained relatively stable, although a gentle decrease and recovery was noted between days 76 and 82, coincident with the sharp change in brightness temperatures.

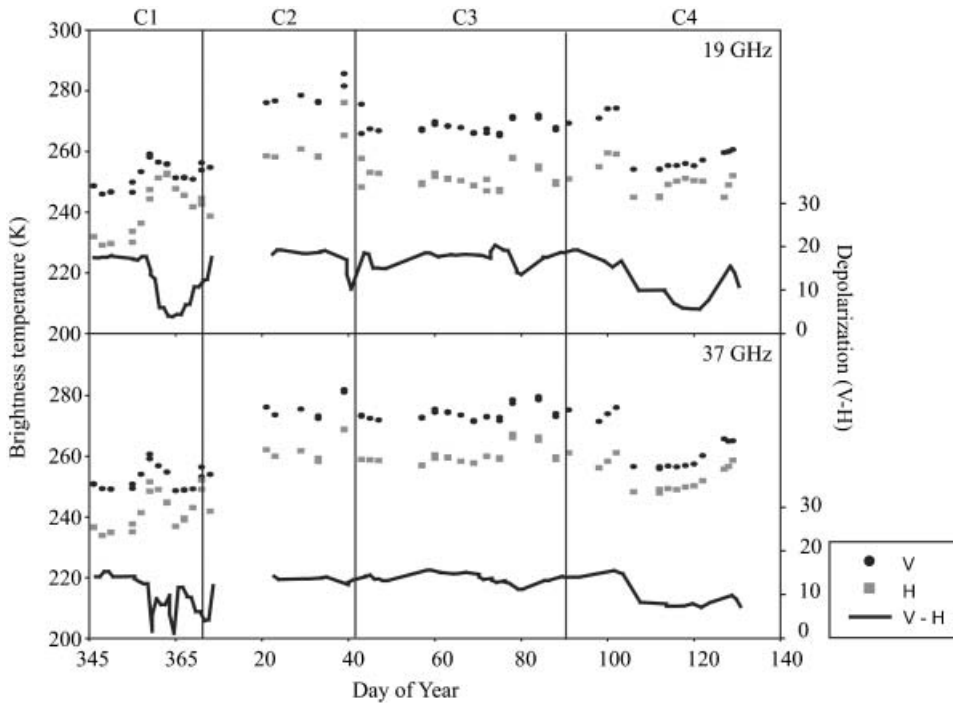


Figure 8. Temporal evolution of brightness temperatures and depolarization for 19 and 37 GHz.

3.2.4 Cluster 4 (C4). During C4, grain size, density, wetness, salinity and brine volume were not measured within the layers from L1 to L4 until day 110 due to flooding of the basal layers (Langlois *et al.* 2007a). Grain size values from L5 to L8 increased at the beginning of the period, then decreased until day 127 (figure 5(a)). Snow density did not follow any particular trend, with values varying around 400 kg m^{-3} in L1, and between 300 and 400 kg m^{-3} in L2 to L6 (figure 5(b)). Temperatures reached a maximum of -4.6 and -7°C in L1 and L3 on day 103 (figure 6(a)), followed by a decrease in all layers between days 110 and 116. High wetness values were recorded between days 118 and 127 (figure 6(b)) although no significant trend was observed. Both salinity and brine volume increased significantly in the early stages of C4, especially at L5 and L6 (figure 7).

The highest ε' values through the vertical profile were measured at L5 between days 95 and 105 (figure 9(a)), but no data were available in the bottom four layers. Relatively high permittivity values were modelled after day 110 for L1 and L2 where the average reached 1.8. The ε'' was negligible from L5 to L8 (figure 9(b)), whereas values in the bottom four layers increased between day 110 and day 120.

A significant drop in T_b was measured between day 100 and 110 when values reached a minimum at all frequencies and polarizations (figure 8). This decrease was the most important of the season with rates of 2.02 and 1.43 K day^{-1} at 19 GHz, and 2.02 and 1.32 K day^{-1} for 37 GHz, for v-pol and h-pol, respectively. The T_b increased slightly thereafter at both frequencies. Depolarization began a slow downward trend in C4, although there was some recovery in the 19 GHz channel after day 120.

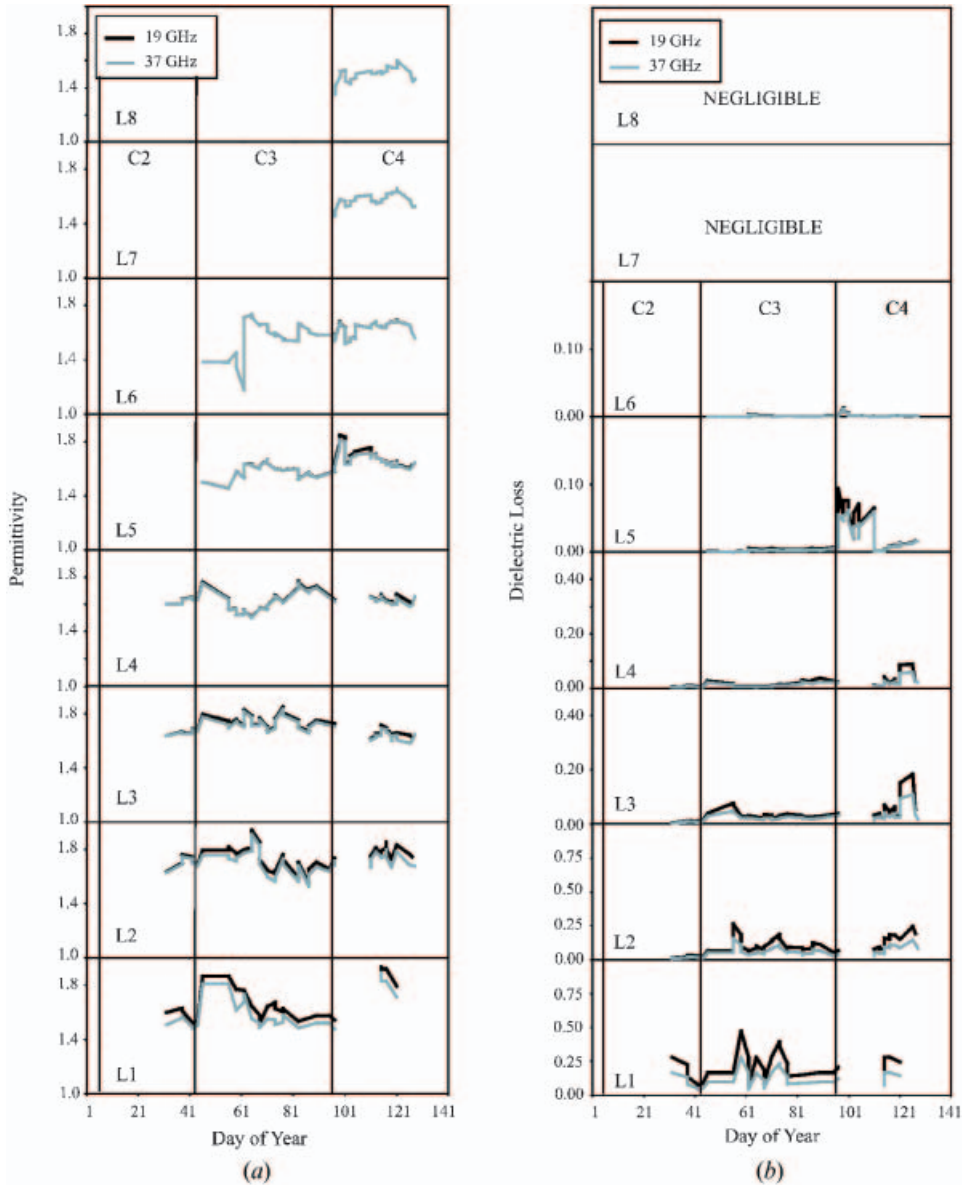


Figure 9. Temporal evolution of snow (a) permittivity and (b) dielectric loss for both 19 and 37 GHz.

3.3 Discussion

The lower brightness temperatures for C1 depicted in figure 8 are a result of very high salinity values throughout the snow cover (figure 7(a)). Salinity contributes to high values of permittivity (not measured for this period), masking the emission from the layers below (Garrity 1992). The decrease in salinity through C1 affected the depolarization (decrease), as shown in figure 8 (Mätzler 1987). Snow cover, although thin, is very dense due to the combined action of wind and equilibrium metamorphism that sinters the snow grains together in the absence of a strong

temperature gradient (Colbeck 1982). Such a dense layer decreases the ability of the medium to permit the incident microwave radiation from below (e.g. Mätzler 1987, Hallikainen 1989, Comiso *et al.* 1989, Lohanick 1993, Barber *et al.* 1994, Pulliainen and Hallikainen 2001), decreasing the overall T_b .

In C2, the increase in brightness temperatures in both 19 and 37 GHz was due to a combination of many factors. First, this period was marked by an abrupt end to the desalination process (figure 7(a)) that decreased the overall dielectric constant of the snow cover (dielectric data are limited for this period). Previous work by Langlois *et al.* (2007a) showed a desalination rate throughout C1 of -0.12 ppt day⁻¹ and stable values through C2. Furthermore, the thickening snow cover raised the overall volume temperature and wetness of the snowpack, thereby increasing the emission at both frequencies (e.g. Foster *et al.* 1984, Mätzler and Huppi 1989, Walker and Goodison 1993, Hwang *et al.* 2007).

The slight decrease in T_b during the earlier stages of C3 was attributed to grain growth (figure 5(a)) caused by an increase in available water vapour (warming temperatures) and a large temperature gradient in the snow pack. The volume scattering triggered by such grain growth changed the temporal evolution of T_b and was also coincident with the transition between the winter cooling and warming periods (see Langlois *et al.* 2007a). This transition occurred when the snow depth reached a thickness of 24 cm (SWE: 33 mm), a very important aspect in estimating SWE from passive microwaves (§4.0). In addition, the increasing thickness of the snowpack was reflected in rising densities in the top and middle layers, a change that had a direct effect on the permittivity and dielectric loss at L5 (figure 9(a) and (b)).

Continuing increases in snowpack thickness and grain size (volume scattering) caused the decrease in T_b measured in C4 (figure 8). Concordant with increasing temperatures, the increased liquid fraction throughout the snow cover vertical profile in turn increased the density and permittivity in L5 (Lohanick 1993, Grody and Basist 1996, Sokol *et al.* 1999, Rosenfeld and Grody 2000). Since the wetness increase was measured at the bottom of the snow cover, the volume scattering from overlying snow layers was the dominant process that caused the T_b to decrease given the penetration depth.

4. Algorithm development

Multiple regression-based SWE algorithms commonly use air and/or volume temperature data to drive the statistical process. Previous work found best results using the snow–ice interface temperature data (Barber *et al.* 2003) because of its effect on the brine volume fraction, a factor that plays a significant role in microwave scattering and emission mechanisms. Langlois *et al.* (2007b) obtained even better predictions over varying snow thicknesses using only air temperatures. We tested multiple regressions on two cases (C1 and C2 during the cooling period vs C3 and C4 during the warming period given figure 4) to see which of T_{air} (air temperature), T_{si} (snow–ice interface temperature) or $T_{\text{air}} - T_{\text{si}}$ (temperature difference between air and snow–ice interface) is most appropriate to drive a seasonal SWE algorithm.

Both C1 and C2 brightness temperatures increased with increasing SWE, whereas C3 and C4 T_b decrease with increasing SWE. The ‘switch’ occurred between C2 and C3 at a median thickness value of 24 cm (33 mm of SWE). Using a similar methodology, we applied multiple regression on C1 and C2 separately from C3 and

C4 using one of air, surface, or snow/ice interface temperatures along with the SWE as independent variables (table 1) and a combination of frequency and polarization as the dependent variable.

In general, better-fit results were found during C1 and C2 using the vertical polarization signal at both 19 and 37 GHz. For thin snow, the 19 GHz v-pol signal with T_{air} gives the best results whereas results in thicker snow were best using the 37 GHz v-pol signal with T_{air} . A significant relationship was also found using the $T_{\text{air}} - T_{\text{si}}$ gradient but T_{air} is much easier to retrieve from weather station or satellite datasets. Our best-fit SWE prediction algorithm becomes:

$$\text{SWE} = \frac{T_{\text{b-19V}} - 0.24T_{\text{air}} - 219.54}{2.29} \quad (1)$$

for $0 < \text{SWE} < 33$ mm, $-30.3 < T^{\circ} < -5^{\circ}\text{C}$ and $246 < T_{\text{b}} < 288$ K and

$$\text{SWE} = \frac{T_{\text{b-37V}} - 0.24T_{\text{air}} - 219.54}{2.29} \quad (2)$$

for $33 < \text{SWE} < 55$ mm, $-30.3 < T^{\circ} < -5^{\circ}\text{C}$ and $256 < T_{\text{b}} < 280$ K.

The pair of algorithms accumulate snow using equation (1) until SWE reaches 33 mm at which point it switches to equation (2), valid up to 55 mm. This range of application is typical of snow thickness distributions on first-year sea ice (Iacozza and Barber 2001). Coupling our algorithms to the annual *in situ* measurements, we obtained a correlation (R^2) of 0.95 for the period from December to May. These results provide a significant improvement over previous research in the range for which the algorithms are valid. The predicted values are shown in figure 10 for a typical snow thickness evolution of 0.50 cm day^{-1} between days 344 and 127 with air temperatures below -5°C throughout the period.

5. Comparison with other algorithms

We compared our results with other SWE prediction algorithms published in the literature. We focused on two algorithms that apply to *in situ* measurements of snow over sea ice (Barber *et al.* 2003 and Langlois *et al.* 2007b) and two for satellite measurements (Cavalieri and Comiso 2004, Markus *et al.* 2006).

Table 1. Coefficient of determination between air, surface, snow–ice interface temperatures and temperature gradient with 19 and 37 GHz for (a) C1 and C2 periods and (b) C3 and C4 periods. Multiple regression R^2 values are given.

	T_{air}	T_{s}	T_{si}	$T_{\text{air}} - T_{\text{si}}$
(a) C1 and C2				
19V	0.81	0.80	0.80	0.81
19H	0.61	0.61	0.59	0.65
37V	0.81	0.80	0.79	0.80
37H	0.77	0.76	0.72	0.78
(b) C3 and C4				
19V	0.75	0.75	0.74	0.75
19H	0.13	0.13	0.13	0.22
37V	0.80	0.80	0.80	0.81
37H	0.67	0.67	0.66	0.68

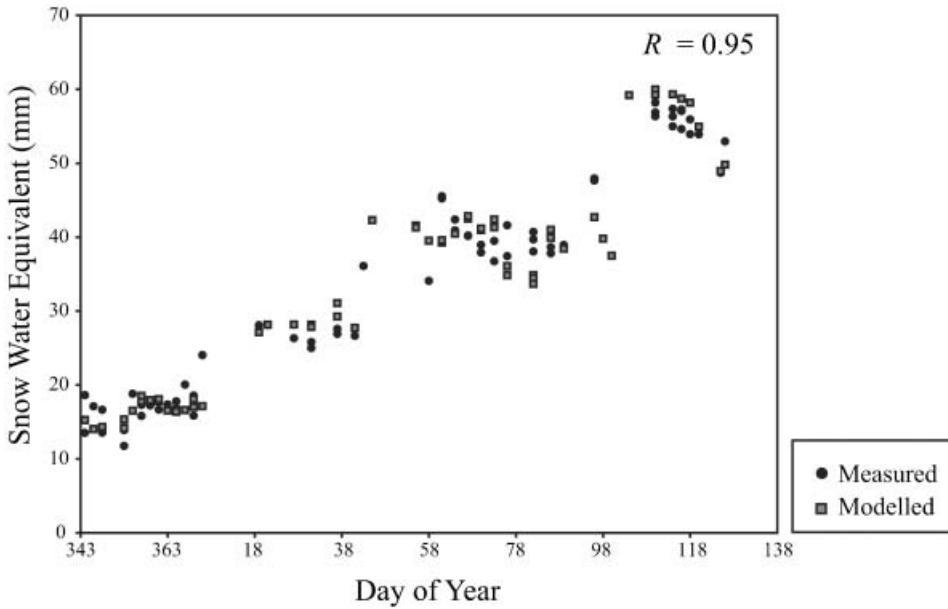


Figure 10. Correlation between measured and modelled snow water equivalent (SWE).

5.1 Barber et al. (2003)

The authors also used a multiple regression solution based on temperatures to produce a prediction of SWE. Interestingly, they too found better results using a single frequency and polarization (37 GHz, h-pol) based on the surface-based radiometer data so that:

$$\text{SWE} = \frac{T_{b-37\text{H}55} - 264.301 - 0.726T_{\text{air}}}{0.014}. \quad (3)$$

We obtained poor results after testing this algorithm against our *in situ* measurements of SWE. The algorithm was most accurate during C2 and C3 only in the range of snow thicknesses for which it was developed. Predictions underestimated measured SWE by approximately 50% throughout C2 and C3.

The shortcomings observed are likely due to the short seasonal development of the algorithm, conducted between 29 April and 8 May when snow thickness varied between 9 and 29 cm. It is for reasons such as this that this work focuses on the whole seasonal evolution of the snowpack, valid over a variety of snow thickness and air temperatures, encompassing the period used in Barber *et al.* (2003).

5.2 Langlois et al. (2007b)

In Langlois *et al.* (2007b), the authors obtained their most significant results by also distinguishing between thin and thick snow cover but no threshold value was identified. We applied their thin snow SWE algorithm to C1 and C2 as:

$$\text{SWE}_{\text{THIN}} = \frac{(T_{b-19\text{H}40} - 277.01 - 0.57T_{\text{air}})}{-1.15} \quad (4)$$

where T_{b19H40° are the brightness temperatures at 19 GHz h-pol at 40° incidence angle. When using this algorithm at the Brewster angle, we obtained reasonable results, with an R^2 of 0.68. The algorithm overestimated C1 SWE (by approximately 31%) and dramatically underestimated those in C2.

$$\text{SWE}_{\text{THICK}} = \frac{(T_{b-19H55^\circ} - 235.33 - 0.43T_{\text{air}})}{0.1} \quad (5)$$

When applying the thick snow algorithm (to C3 and C4), we also obtained poor results due to the limited range of thicknesses upon which the algorithm was based. The predicted values overestimated our measured values by a factor of 10. Furthermore, the incidence angle in their study was different than the one in this work, a complication that can cause significant differences in the brightness temperatures, especially in the warmer period (e.g. Tiuri *et al.* 1984, Eppler 1992, Powell *et al.* 2006).

5.3 Markus *et al.* (2006)

Markus *et al.* (2006) used satellite-based AMSR-E (Advanced Microwave Scanning Radiometer – EOS) brightness temperatures accounting for ice (T_{b-ICE}) and open-water (T_{b-OW}) brightness temperatures and ice concentration (C) (Markus and Cavalieri 2000):

$$T_{b-SAT} = CT_{b-ICE} + (1 - C)T_{b-OW}. \quad (6)$$

In our case, the sampling area was located in a smooth pan of landfast first-year sea ice (Langlois *et al.* 2007a), which covered 100% of the Franklin Bay region so that:

$$T_{b-SAT} = T_{b-ICE}. \quad (7)$$

In Markus *et al.* (2006), the spectral-ratio difference in brightness temperatures between 19 and 37 GHz (gradient ratio, GR) in the vertical polarization was analysed, such that the spectral ratio of sea ice is equal to the spectral ratio measured at the satellite scale ($\text{GR}_{ICE} = \text{GR}$) from equation (8):

$$\text{GR} = \frac{T_{b-37V} - T_{b-19V}}{T_{b-37V} + T_{b-19V}} \quad (8)$$

Snow depth (h_s) in cm was then retrieved using:

$$h_s = 2.9 - 782 \times \text{GR}. \quad (9)$$

The coefficients in equation (9) are from the AMSR-E sensor (Comiso 2003). This algorithm was developed in the Antarctic so that it can only be applied over first-year sea ice in the Arctic due to the similar brightness temperatures signatures between multi-year sea ice and deep snow. When we applied this equation to our *in situ* measurements, we obtained poor thickness predictions, with negative values in 56% of the cases. Otherwise, the algorithm dramatically underestimated thickness in all C1, C2, C3 and C4 periods, confirming the observation that brightness

temperature difference is not appropriate over first-year sea ice (Armstrong and Brodzik 2001, Barber *et al.* 2003, Foster *et al.* 2005, Langlois *et al.* 2007b).

5.4 Cavalieri and Comiso (2004)

Another satellite-based algorithm, developed by Cavalieri and Comiso (2000), also used equations (7) and (8), but with different coefficients. Snow depth was retrieved using:

$$h_s = -2.34 - 771 \times \text{GR}. \quad (10)$$

This algorithm did not perform better than the algorithm developed by Markus *et al.* (2006), with negative thickness values in 84% of our measurements and a greater underestimation in the positive values. Again, these algorithms were developed using AMSR-E brightness temperature data that can be significantly different than SBR measurements due to the contribution of various spatial features in a 12.5 km pixel compared to the protected area where our measurements occurred. This issue of mixed-pixel measurements is a subject of current and future work.

6. Conclusions

6.1 Evaluate the impact on in situ passive microwave signatures

In this paper, we evaluated the impact of seasonal snow thermophysical properties on the brightness temperatures at an incidence angle of 53° for both 19 and 37 GHz. We found that the seasonal pattern in T_b was quite different given the seasonally variable thermal regime that affects snow thermodynamic processes such as kinetic growth. During the first half of the winter (C1 and C2), T_b was dictated by the desalination process, as thickness did not yet play an important role in volume scattering. In the latter part of the winter, significant changes occurred in the snow with increasing grain growth and consequent volume scattering. As temperatures rose, the amount of liquid water in the upper part of the snow cover increased the permittivity, which decreased the emissivity contribution of the bottom part of the snowpack (decrease in T_b).

6.2 Develop a seasonal SWE algorithm valid over the typical range of snow thickness evolution over first-year smooth ice

We developed a seasonal SWE retrieval algorithm over first-year sea ice valid from 0 to 55 mm for a temperature range between -30.3 and -5°C . Previous research showed that different snow thicknesses behave quite differently thermodynamically, thereby affecting the snow microwave emissivity. For an evolving snow cover, we identified a snow thickness at which a different algorithm is needed to retrieve SWE prediction values (33 mm of SWE). The combination of both algorithms was necessary and provided a seasonal SWE prediction R^2 of 0.95. This is a significant advance over previous results and is currently the only seasonally valid SWE algorithm for application over first-year sea ice. However, limitations exist due to the unique dataset. The algorithm was developed over one area throughout one winter season. Year-to-year comparison is required in multiple areas in order to make the algorithm applicable over all the first-year sea ice located in the Arctic from a satellite remote sensing perspective.

6.3 Compare this algorithm with existing satellite sensor data

We compared our algorithm with existing *in situ* and satellite products and achieved superior results. The main shortcoming of previous work seems to be due to the limited thickness and temperature ranges over which earlier algorithms were developed. Furthermore, the satellite algorithms are constrained by large $12.5 \text{ km} \times 12.5 \text{ km}$ pixels that, in addition to the spatial variability of snow thickness, encompasses a variety of spatial features such as ice ridges and re-frozen leads. Further complications in the use of satellite sensor data arise from the radiometry physics that must account for such factors as the atmospheric upwelling and downwelling contributions on T_b (e.g. Kerr and Njoku 1990, Mätzler 1992).

Further work is required to examine satellite remote sensing algorithms with the goal of comparing such algorithms against measured *in situ* data. Our laboratory possesses multiple datasets of snow depth and SWE over first-year sea ice, and over ridges of different amplitude. The algorithm developed in this work was applied to AMSR-E satellite data and compared with other satellite products and provided discussion on sea-ice roughness impact on SWE predictions (Langlois *et al.*, submitted). Microwave snow remote sensing has proven to be the best tool for the development of regional–global scale climate studies; although spatial variation in snow thickness is still one of the main challenges in global SWE retrievals. Currently, the estimation of the scaling exponents of power law is achieved by the employment of the detrended fluctuation analysis, which has already proved its usefulness in several complex systems such as the surface air pollutants (Varotsos 2005, Varotsos and Kirk-Davidoff 2006) and numerous avalanche studies (e.g. Birkeland and Landry 2002). The power-law approach can help estimate the spatial fraction of land-covered snow (e.g. Shook 1993, 1995; Rosenthal and Dozier 1996, Bahr and Meier 2000), and a thorough seasonal analysis should be conducted over first-year sea ice looking at snow thickness spatial variability. In the context of climate change, this approach would greatly help global SWE algorithms, and further climate models.

Acknowledgements

This work was financially supported by grants to DGB for the CASES NSERC network, the Canada Foundation for Innovation (CFI) and the Polar Continental Shelf Project. We would like to thank Christina Blouw, Teresa Fisico, Owen Owens, John Iacozza from the University of Manitoba and Mark Christopher Fuller and Kris Konig for tremendous assistance in the field sampling. Many thanks also to Tim Papakyriakou from the University of Manitoba and John Yackel from the University of Calgary for guidance and support throughout the experiment. The authors would also like to thank the crew of the CCGS Amundsen for an essential logistical support throughout the study.

References

- ACIA (ARCTIC CLIMATE IMPACT ASSESSMENT), 2004, *Impacts of a Warming Arctic* (Cambridge: Cambridge University Press).
- ARMSTRONG, R.L. and BRODZIK, M.J., 2001, Recent northern hemisphere snow extent: a comparison of data derived from visible and microwave satellite sensors. *Geophysical Research Letters*, **28**, pp. 3673–3676.
- ASMUS, K. and GRANT, C., 1999, Surface Based Radiometer (SBR) Data Acquisition System. *International Journal of Remote Sensing*, **20**, pp. 3125–3129.

- BAHR, D.B. and MEIER, M.F., 2000, Snow patch and glacier size distribution. *Water Resources Research*, **36**, pp. 495–501.
- BARBER, D.G. and HANESIAK, J.M., 2004, Meteorological forcing of sea ice concentrations in the southern Beaufort Sea over the period 1979 to 2000. *Journal of Geophysical Research*, **109**, C06014, doi:10.1029/2003JC002027.
- BARBER, D.G. and THOMAS, A., 1998, The influence of cloud cover on the radiation budget, physical properties and microwave scattering coefficient of first-year and multi-year sea ice. *IEEE Transactions on Geoscience and Remote Sensing*, **36**, pp. 38–50.
- BARBER, D.G., PAPAKYRIAKOU, T.N. and LEDREW, E.F., 1994, On the relationship between energy fluxes, dielectric properties, and microwave scattering over snow covered first-year ice during the spring transition period. *Journal of Geophysical Research*, **99**, pp. 22401–22411.
- BARBER, D.G., PAPAKYRIAKOU, T.N., LEDREW, E.F. and SHOKR, M.E., 1995, An examination of the relation between the spring period evolution of the scattering coefficient and radiative fluxes over landfast sea-ice. *International Journal of Remote Sensing*, **16**, pp. 3343–3363.
- BARBER, D.G., IACOZZA, J. and WALKER, A., 2003, Estimation of snow water equivalent using microwave radiometry over Arctic first-year sea ice. *Hydrological Processes*, **17**, pp. 3503–3517.
- BIRKELAND, K.W. and LANDRY, C.C., 2002, Power-laws and snow avalanches. *Geophysical Research Letters*, **29**, 10.1029/2001GL014623.
- CAVALIERI, D. and COMISO, J., 2004, updated daily. *AMSR-ElAqua Daily L3 12.5 km Tb, Sea Ice Concentration, & Snow Depth Polar Grids V001*, March to June 2004 (Boulder, CO, USA: National Snow and Ice Data Center) Digital media.
- CAVALIERI, D. and COMISO, J., 2000, *Algorithm Theoretical Basis Document for the AMSR-E Sea Ice Algorithm, Revised December 1* (Landover, MD: Goddard Space Flight Center).
- CHANG, A.T.C., FOSTER, J.L., HALL, D.K., RANGO, A. and HARTLINE, B.K., 1982, Snow water equivalent estimation by microwave radiometry. *Cold Regions Science and Technology*, **5**, pp. 259–267.
- COLBECK, S.C., 1982, An overview of seasonal snow metamorphism. *Reviews of Geophysics and Space Physics*, **20**, pp. 45–61.
- COMISO, J.C., 2003, Large-scale characteristics and variability of the global sea ice cover. In *Sea Ice: An Introduction to its Physics, Chemistry, Biology and Geology*, D.N. Thomas and G.S. Dieckmann (Eds), pp. 112–142 (Oxford, UK: Blackwell Science).
- COMISO, J.C., GRENFELL, T.C., BELL, D.L., LANGE, M.A. and ACKLEY, S.F., 1989, Passive microwave *in-situ* observations of winter Wedell sea ice. *Journal of Geophysical Research*, **95**, pp. 10891–10905.
- CURRY, J.A., ROSSOW, W.B., RANDALL, D. and SCHRAMM, J.L., 1996, Overview of Arctic cloud and radiation characteristics. *Journal of Climate*, **9**, pp. 1731–1764.
- DRINKWATER, M.R. and CROCKER, G.B., 1988, Modeling changes in the dielectric and scattering properties of young snow-covered sea ice at GHz frequencies. *Journal of Glaciology*, **34**, pp. 274–282.
- DROBOT, S.D. and BARBER, D.G., 1998, Towards development of a snow water equivalence (SWE) algorithm using microwave radiometry over snow covered first-year sea ice. *Photogrammetric Engineering & Remote Sensing*, **64**, pp. 414–423.
- EICKEN, H., 2003, From the microscopic, to the macroscopic, to the regional scale: growth, microstructure and properties of sea ice. In *Sea Ice: An Introduction to Its Physics, Chemistry, Biology and Geology*, D.N. Thomas and G.S. Dieckmann (Eds), pp. 22–81 (Oxford, UK: Blackwell Science).
- EPPLER, D.T., 1992, Passive microwave signatures of sea ice. In *Microwave Remote Sensing of Sea Ice*, F. Carsey (Ed.), pp. 47–71 (Washington, D.C.: American Geophysical Union).

- FISICO, T., 2005, *Section 3.3, Meteorological Observations*, in A. Langlois, T. Fisico, R. Galley and D.G. Barber (Eds), CASES 2003–2004 Field Summary, CEOS-TEC-2004-09-01, 70–110.
- FOSTER, J.L., SUN, C., WALKER, J.P., KELLY, R., CHANG, A., DONG, J. and POWELL, H., 2005, Quantifying the uncertainty in passive microwave snow water equivalent observations. *Remote Sensing of Environment*, **94**, pp. 187–203.
- FOSTER, J.L., HALL, D.K., CHANG, A.T.C. and RANGO, A., 1984, An overview of passive microwave snow research and results. *Reviews of Geophysics*, **22**, pp. 195–208.
- FRANCIS, J.A., HUNTER, E., KEY, J.R. and WANG, X., 2005, Clues to variability in Arctic minimum sea ice extent. *Geophysical Research Letters*, **32**, L21501.
- GARRITY, C., 1992, Characterization of snow on floating ice and case studies of brightness temperature changes during the onset of melt. In *Microwave Remote Sensing of Sea Ice*, F. Carsey (Ed.), pp. 313–328 (Washington, DC: American Geophysical Union).
- GERDES, R., 2006, Atmospheric response to changes in Arctic sea ice thickness. *Geophysical Research Letters*, **33**, L18709.
- GRENFELL, T.C. and MAYKUT, G.A., 1977, The optical properties of ice and snow in the Arctic Basin. *Journal of Glaciology*, **18**, pp. 445–463.
- GRODY, N. and BASIST, A., 1996, Global identification of snow cover using SSM/I measurements. *IEEE Transaction on Geoscience and Remote Sensing*, **34**, pp. 237–249.
- HALLIKAINEN, M.T., 1989, Microwave radiometry of snow. *Advances in Space Research*, **9**, pp. 267–275.
- HOLLAND, M.M. and BITZ, C.M., 2003, Polar amplification of climate change in coupled models. *Climate Dynamics*, **21**, pp. 221–232.
- HWANG, B.J., LANGLOIS, A., BARBER, D.G. and PAPAKYRIAKOU, T.N., 2007, Detection of the thermophysical state of landfast first-year sea ice using *in-situ* microwave emission during spring melt. *Remote Sensing of Environment*, **11**, pp. 148–159.
- IACOZZA, J. and BARBER, D.G., 2001, Ablation patterns of snow cover over smooth first-year sea ice in the Canadian Arctic. *Hydrological Processes*, **15**, pp. 3559–3569.
- IPCC (INTERGOVERNMENTAL PANEL ON CLIMATE CHANGE), 2001, *Climate Change 2001: The Scientific Basis, Contribution of Working Group I to the Third Assessment Report of the Intergovernmental Panel on Climate Change* (New York: Cambridge University Press).
- KELLY, R., CHANG, A.T.C., TSANG, L. and FOSTER, J., 2003, A prototype AMSR-E global snow area and snow depth algorithm. *IEEE Transactions on Geoscience and Remote Sensing*, **41**, pp. 230–242.
- KERR, Y.H. and NJOKU, E.G., 1990, A semi empirical model for interpreting microwave emission from semiarid land surfaces as seen from space. *IEEE Transactions on Geoscience and Remote Sensing*, **28**, pp. 384–393.
- LANGLOIS, A., MUNDY, C.J. and BARBER, D.G., 2007a, On the winter evolution of snow thermophysical properties over landfast first-year sea ice. *Hydrological Processes*, **21**, pp. 705–716.
- LANGLOIS, A., BARBER, D.G. and HWANG, B.J., 2007b, Development of a winter snow water equivalent algorithm using *in-situ* passive microwave radiometry over snow covered first-year sea ice. *Remote Sensing of Environment*, **106**, pp. 75–88.
- LANGLOIS, A., SCHARIEN, R., GELSETZER, T., IACOZZA, J., BARBER, D.G. and YACKEL, J., submitted, Estimating snow water equivalent over first-year sea ice using satellite microwave remote sensing. *Remote Sensing of Environment*.
- LEDLEY, T.S., 1991, Snow on sea ice: competing effects in shaping climate. *Journal of Geophysical Research*, **96**, pp. 17 195–17 208.
- LOHANICK, A.W., 1993, Microwave brightness temperatures of laboratory-grown undeformed first-year ice with an evolving snow cover. *Journal of Geophysical Research*, **98**, pp. 4667–4674.
- MARKUS, T. and CAVALIERI, D.J., 2000, An enhancement of the NASA Team sea ice algorithm. *IEEE Transactions on Geoscience and Remote Sensing*, **38**, pp. 1387–1398.

- MARKUS, T., POWELL, D.C. and WANG, J.R., 2006, Sensitivity of passive microwave snow depth retrievals to weather effects and snow evolution. *IEEE Transactions on Geoscience and Remote Sensing*, **44**, pp. 68–77.
- MARTIN, C.F., THOMAS, R.H., KRABILL, W.B. and MANIZADE, S.S., 2005, ICESat range and mounting bias estimation over precisely-surveyed terrain. *Geophysical Research Letters*, **32**, L21S07.
- MÄTZLER, C., 1987, Applications of the interaction of microwaves with natural snow cover. *Remote Sensing Reviews*, **2**, pp. 259–387.
- MÄTZLER, C. and HUPPI, R., 1989, Review of signatures studies for microwave remote sensing of snow packs. *Advances in Space Research*, **9**, pp. 253–265.
- MÄTZLER, C., 1992, Passive microwave signature catalogue 1989–1992. Report, Vol. 1, Institute of Applied Physics, University of Berne.
- POLYAKOV, I.V., ALEKSEEV, G.V., BEKRYAEV, R.V., BHATT, U.S., COLONY, R., JOHNSON, M.A., KARKLIN, V.P., WALSH, D. and YULIN, A.V., 2003, Long-term ice variability in arctic marginal seas. *Journal of Climate*, **16**, pp. 2078–2085.
- POWELL, D.C., MARKUS, T., CAVALIERI, D.J., GASIEWSKI, A.J., KLEIN, M., MASLANIK, J.A., STROEVE, J.C. and STURM, M., 2006, Microwave signatures of snow on sea ice. *IEEE Transactions on Geoscience and Remote Sensing*, **44**, pp. 3091–3102.
- PULLIAINEN, J. and HALLIKAINEN, M., 2001, Retrieval of regional snow water equivalent from space-borne passive microwave observations. *Remote Sensing of Environment*, **75**, pp. 76–85.
- ROSENFELD, S. and GRODY, N., 2000, Anomalous microwave spectra of snow cover observed from Special Sensor Microwave Imager measurements. *Journal of Geophysical Research*, **105**, pp. 14913–14925.
- ROSENTHAL, W. and DOZIER, J., 1996, Automated mapping of montane snow cover at subpixel resolution from the Landsat Thematic Mapper. *Water Resources Research*, **32**, pp. 115–130.
- ROTHROCK, D.A. and ZHANG, J., 2005, Arctic Ocean sea ice volume: what explains its recent depletion? *Journal of Geophysical Research*, **110**, C01002.
- SERREZE, M.C., MASLANIK, J.A., SCAMBOS, T.A., FETTERER, F., STROEVE, J., KNOWLES, K., FOWLER, C., DROBOT, S., BARRY, R.G. and HARAN, T.M., 2003, A record minimum arctic sea ice extent and area in 2002. *Geophysical Research Letters*, **30**, p. 1110.
- SHOOK, K., 1993, Fractal geometry of snowpacks during ablation. MSc thesis, University of Saskatchewan, Saskatoon, Canada.
- SHOOK, K., 1995, Simulation of the ablation of prairie snowcovers. PhD thesis, University of Saskatchewan, Saskatoon, Canada.
- SINGH, P.R. and GAN, T.Y., 2000, Retrieval of snow water equivalent using passive microwave brightness temperature data. *Remote Sensing of Environment*, **74**, pp. 275–286.
- STROEVE, J.C., SERREZE, M.C., FETTERER, F., ARBETTER, T., MEIER, W., MASLANIK, J. and KNOWLES, K., 2005, Tracking the Arctic's shrinking ice cover: another extreme minimum in 2004. *Geophysical Research Letters*, **32**, L04501.
- STURM, M., HOLMGREN, J. and PEROVICH, D.K., 2002, Winter snow cover on the sea ice of the Arctic ocean at the Surface Heat Budget of the Arctic Ocean (SHEBA): temporal evolution and spatial variability. *Journal of Geophysical Research*, **107**, p. 8047.
- TIURI, M.E., SIHVOLA, A.H., NYFORS, E.G. and HALLIKAINEN, M.T., 1984, The complex dielectric constant of snow at microwave frequencies. *IEEE Journal of Oceanic Engineering*, **OE-9**, pp. 377–382.
- TSANG, L. and KONG, J.A., 1992, Scattering of electromagnetic waves from a dense medium consisting of correlated Mie scatterers with size distributions and applications to dry snow. *Journal of Electromagnetic Waves and Applications*, **6**, pp. 265–286.
- ULABY, F.T., MOORE, R.K. and FUNG, A.K., 1986, *Microwave Remote Sensing* (Norwood, MA: Artech House).
- VAROTSOS, C., 2005, Power-law correlations in column ozone over Antarctica. *International Journal of Remote Sensing*, **26**, pp. 3333–3342.

- VAROTSOS, C. and KIRK-DAVIDOFF, D., 2006, Long-memory processes in ozone and temperature variations at the region 60 degrees S–60 degrees N. *Atmospheric Chemistry and Physics*, **6**, pp. 4093–4100.
- WALKER, A. and GOODISON, B., 1993, Discrimination of a wet snow cover using passive microwave satellite data. *Annals of Glaciology*, **17**, pp. 307–311.
- WARREN, S.G., RADIONOV, V.F., BRYAZGIN, N.N., ALEKSANDROV, Y.I. and COLONY, R., 1999, Snow depth on Arctic sea ice. *Journal of Climate*, **12**, pp. 1814–1829.
- YU, Y., MAYKUT, G.A. and ROTHROCK, D.A., 2004, Changes in the thickness distribution of Arctic sea ice between 1958–1970 and 1993–1997. *Journal of Geophysical Research*, **109**, C08004.